Surface Science Reports 64 (2009) 1–45

Contents lists available at ScienceDirect

Surface Science Reports

journal homepage: www.elsevier.com/locate/surfrep

Surface reactivity of pyrite and related sulfides

Riley Murphy, Daniel R. Strongin *

Department of Chemistry, Temple University, Philadelphia, PA 19122, United States

ARTICLE INFO

Article history:
Accepted 27 September 2008
editor: J.G. Chen

Keywords:
Pyrite
Iron sulfides
Surface defects
Photoelectron spectroscopy
Metal sulfide oxidation

ABSTRACT

Pyrite, FeS_2, commonly referred to as "Fool's gold" is the most common sulfide in the Earth's surface region. Not only is the mineral ubiquitous, but the reactivity of pyrite is of central importance in a devastating environmental issue known as acid mine drainage (AMD) and in beneficial commercial processes such as mineral benefaction, which can range from the desulfurization of coal to the isolation of copper or gold ores. Pyrite has even been postulated to be a key constituent of a prebiotic iron–sulfur world existing at the high pressure and temperature conditions common to hydrothermal vents at the oceanic floor. The development of an atomic level picture of the structure and reactivity of pyrite is paramount to understanding the chemistry of this mineral in these wide-ranging environments.

This contribution focuses on research carried out over the past three decades that has used modern surface science tools to understand the reactivity of pyrite surfaces. An understanding of the reactivity of the pyrite surfaces has benefited from studies using a wide range of experimental techniques that range from vacuum-based experiments utilizing electron and photon spectroscopies, and probe microscopy to in situ studies using infra-red spectroscopy. Synchrotron-based techniques that include photoelectron spectroscopy and X-ray absorption spectroscopy have played a large role in both these environments. These techniques have perhaps been the most useful in establishing the structure of the pristine pyrite surface. Related iron sulfides are also briefly introduced in this review including pyrrhotite (Fe_xS_{1-x}) and the dimorph of pyrite, marcasite. The surface reactivity of these sulfides exhibit both similarities and differences to pyrite, and help to bring forward the unique activity of pyrite in both environmentally and technologically important conditions.

Contents

* Corresponding author.
E-mail addresses: riley.murphy@temple.edu (R. Murphy), dstrongi@temple.edu (D.R. Strongin).

0167-5729/$ – see front matter © 2008 Published by Elsevier B.V.
doi:10.1016/j.surfrep.2008.09.002

Table of abbreviations

AES	Auger electron spectroscopy
AFM	atomic force microscopy
AMD	acid mine drainage
ATR	attenuated total reflection
DFT	density functional theory
DOS	density of states
EELS	electron energy loss spectroscopy
FTIR	Fourier transform infrared
HOMO	highest occupied molecular orbital
L	Langmuir – (10^{-6} Torr s)
LEED	low energy electron diffraction
LUMO	lowest unoccupied molecular orbital
NEXAFS	near-edge X-ray absorption fine structure
PAX	photoemission of adsorbed xenon
PES	photoelectron spectroscopy
REFLEXAFS	reflection extended X-ray absorption fine structure
SIMS	secondary ion mass spectroscopy
STM	scanning tunneling microscopy
STS	scanning tunneling spectroscopy
TPD	temperature programmed desorption
UPS	ultraviolet photoelectron spectroscopy
XAS	X-ray absorption spectroscopy
XANES	X-ray absorbance near-edge structure
XPS	X-ray photoelectron spectroscopy
XRD	X-ray diffraction
XRF	X-ray fluorescence

1. Introduction

Pyrite (FeS_2), commonly referred to as "Fool's gold", is the most abundant metal sulfide associated with the Earth's surface region. The mineral is ubiquitous to terrestrial sediments and marine environments, including those associated with submarine hydrothermal vents. Rickard and Luther [1] have recently estimated that, simply due to the biogenic reduction of aqueous sulfate, there is about 5 million tons of pyrite being produced annually in the oceanic environment.

Not only does pyrite present itself in many different environments, it exhibits surface chemistry that can profoundly affect the very environment in which it is present. Perhaps one of the most striking examples of how the reactivity of pyrite can affect an environment is associated with anthropogenic activities. The oxidative decomposition of pyrite at coal and metal mining sites leads to the devastating environmental problem known as acid mine drainage (AMD) [2–6]. This process, through the generation of sulfuric acid and iron oxyhydroxides, is responsible for the contamination of over 10,000 miles of streams and rivers and 180,000 acres of lakes and reservoirs in the US alone [7]. An estimated 10 million tons of pyrite is disposed of per year by the 6 highest producing states in the US [7]. The remediation of this acidic run-off due to AMD is staggering, costing the coal mining industry 1 million dollars per day in prevention and abatement [8]. Furthermore, the decomposition of pyrite in the environment releases heavy metals such as arsenic, cobalt, lead, nickel, and zinc into neighboring waterways.

The surface chemistry of pyrite (and other sulfides) also plays a large role in the commercially important processes of mineral benefaction [9] and the separation of sulfides from coal. Here a key consideration is the intelligent functionalization of the iron sulfide material in coal/mineral slurries so as to separate coal from sulfides (to limit the production of sulfur oxides during burning that leads to acid rain), or for the separation of valuable and nonvaluable sulfides that contain, for example, copper or gold. Froth flotation is the leading process for the selective separation of sulfides by mass and is a 100 million dollar a year industry, resulting in the processing of 10^9 tons of material each year [9]. The process depends on the modification of the sulfide surface (often pyrite) with organic xanthates or metals such as Cu to make its surface properties (charge, hydrophobicity etc.) amenable to separation.

On a less technologically relevant level, but a very intriguing level nonetheless, the surfaces of iron sulfides have been postulated to facilitate chemistry within active hydrothermal vents, that have been discovered in some deep ocean environments [10,11]. Under such conditions of high pressure and temperature, it has

been shown that particular iron sulfide surfaces facilitate chemistry that would be otherwise associated with metal and/or metal oxide surfaces under heterogeneous catalysis conditions. For example, it has been shown that pyrrhotite (Fe_xS_{1-x}) slurries at high pressure (exceeding 100 MPa) and at elevated temperatures facilitate Fisher Tropsch chemistry [12,13]. Also, it has been shown that under hydrothermal conditions ferrous iron sulfide can catalyze dinitrogen conversion to ammonia [14]. The reaction of iron sulfides under these extreme conditions has also been postulated to be relevant to prebiotic chemistry [10,15].

The development of a microscopic understanding of the molecular controls that determine the surface reactivity of pyrite in the before-mentioned environments has been intimately linked to the development of a sophisticated suite of surface sensitive probes. For example, synchrotron-based techniques and infrared techniques have allowed an unprecedented view of the buried interface that often characterizes the working surface of an environmentally relevant mineral. Such studies have nicely complimented parallel studies over the years that have been restricted to the study of iron sulfides under well-defined vacuum-based conditions. These experimental studies taken together with an ever advancing theoretical framework have led to a deep understanding of this important mineral.

The current contribution will review the progress that is being made via theoretical and experimental efforts focused on investigating the reactivity of pyrite. Emphasis will be placed on the how the surface chemistry exhibited by this mineral is related to particular environmental and industrial processes. The review will highlight how surface speciation, electron transfer, secondary mineral phases, short-range order, and structure sensitivity contribute to the sulfide mineral surface chemistry. Furthermore, the contribution will introduce other iron sulfides such as the dimorph marcasite (FeS_2), pyrrhotite ($Fe_{1-x}S$) and the FeS endmember, troilite, for comparative purposes. Rosso and Vaughan have recently reviewed the surface reactivity of a variety of metal sulfides [16]. While there is some overlap with this earlier contribution, we have tried to restrict our review primarily to pyrite which has allowed us to treat this mineral in somewhat more detail than has been done before. This review will briefly include the influence of microbes (there are more complete reviews on this particular aspect [17]) on these environmental processes for completeness, but will primarily focus on abiotic chemistry.

2. Pyrite structure and samples for surface science studies

2.1. General structure

Pyrite crystallizes in a rock salt type structure (face-centered cubic) and belongs to the space group Pa3 [18]. The mineral adopts a cubic NaCl-like structure with the Fe atoms on the corners and face center positions of the unit cell and the S_2 units lie at the midpoints of the twelve edges and in the center of the cube. The sulfur dimers occupying the anion sites along the ⟨111⟩ directions reduce the crystal symmetry from that of the rock salt structure. The unit cell of pyrite contains four FeS_2 formula units. Fig. 1 shows the pyrite unit cell with full dimers at the midpoint of each edge. The unit cell is completely defined by the cell wall length, or cell parameter, a_0, and the S coefficient, u, which defines the coordinates of each S atom in the unit cell. The crystal structure of pyrite was published in 1914 by Bragg [19], and the parameters are now generally accepted as $a_0 = 5.416$ Å and $u = 0.385$ Å [20,21]. Each Fe is coordinated to six S atoms creating a distorted octahedral field, while each S atom is coordinated to 3 Fe atoms and its dimer partner.

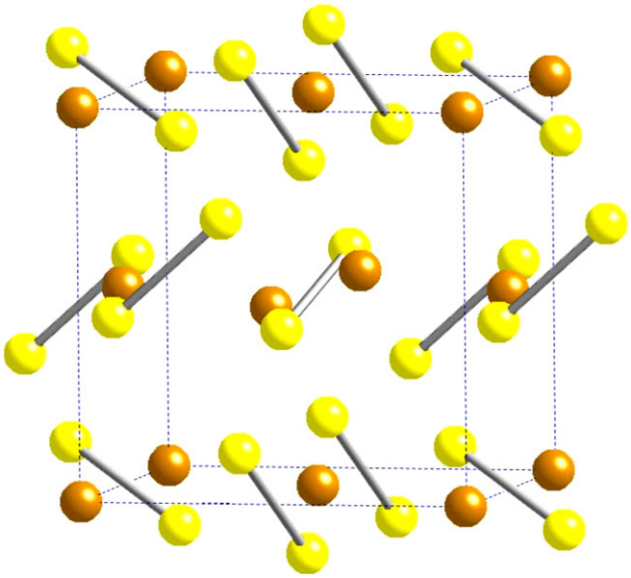

Fig. 1. Atomistic representation of the pyrite unit cell. Brown spheres represent Fe and yellow spheres represent S.

Pyrite cleaves poorly and fractures conchoidally with {100} cleavage being the most common, but {021}, {111} and {110} cleavage is also observed [22]. Growth of the {100} plane forms a cubic structure, while the less common growth in both the {111} and {100} planes creates a cubo-octahedral form while a pyritohedral form is defined by the {210} plane, although other forms have also been reported [23]. Surface science studies have generally been conducted on the pyrite {100} plane, but some studies have addressed the {111} plane and will be presented later. Fig. 2 shows idealized terminations of the pyrite bulk that generate the {100} and {111} planes.

Abraitis et al. [24] have reviewed the types and concentrations of impurities found in natural pyrite. Their analysis shows that natural pyrite (with the overall S:Fe ratio being close to 2) contains a variety of trace Ag, As, Au, Bi, Cd, Co, Cu, Hg, Mo, Ni, Pb, Pd, Ru, Sb, Se, Te, Zn and up to a few % of some elements (e.g., As, Co, Cu). Specific elements can exist as substitutions in the pyrite lattice or as inclusions. Depending on the impurity, the natural pyrite semiconducting mineral can show p-type (typically containing As) or n-type conductivity. Conductivities can range from 0.02 to 562 $(\Omega\ \mathrm{cm})^{-1}$, with the mean conductivities for p and n-type pyrite being 0.5 and 56 $(\Omega\ \mathrm{cm})^{-1}$, respectively [24].

2.2. Types of samples for surface science studies

Surface science studies of the iron sulfides have been carried out on surfaces associated with mineral powder, surfaces resulting from the fracturing of the mineral, as-grown surfaces, and those associated with synthetic thin films. The following will briefly review some aspects of these different samples.

2.2.1. Powder or crushed iron sulfide

Studies involving the use of pyrite powder have generally been confined to investigations concerned with the rate of pyrite oxidation in various oxidizing environments and in experiments that have investigated the chemistry of the sulfide under hydrothermal conditions. Rate measurements of pyrite oxidation typically involve the measurement of aqueous sulfate and iron and such measurements are aided by the relatively high surface area afforded by crushed pyrite.

In the realm of surface science studies, crushed pyrite has been shown to be particularly convenient for attenuated total reflection

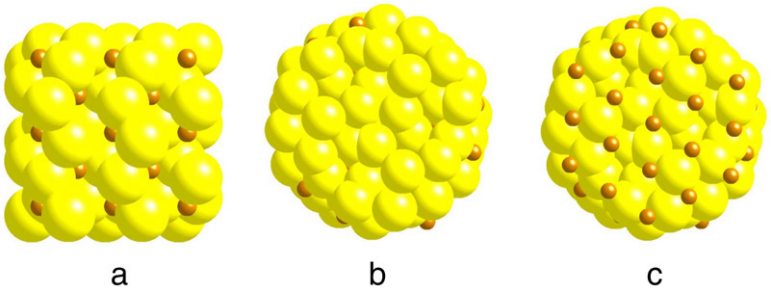

Fig. 2. Ideal planes of FeS_2 (a) S-terminated {100}, (b) S-terminated {111}, and (c) Fe terminated {111}. Brown spheres represent Fe and yellow spheres represent S.

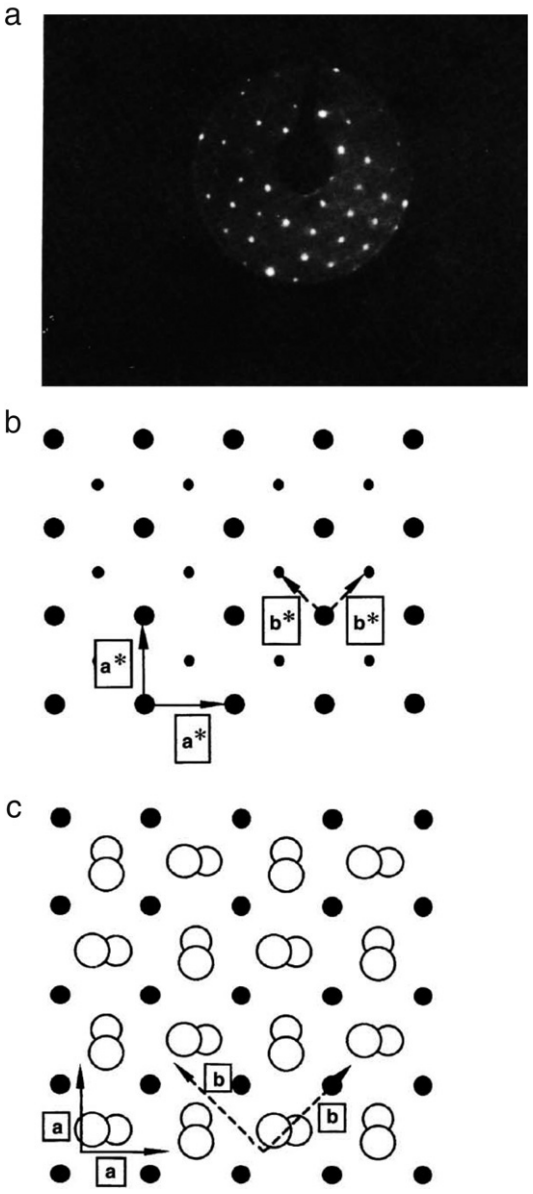

Fig. 3. (a) LEED diffraction pattern of FeS_2 (100) cleavage planes. (b) Schematic representation of the reciprocal lattice of the (100) plane (a* reciprocal lattice vector of the Fe fcc sublattice, b* of the S_2 superstructure). (c) Atomic arrangement within the (100) plane (a, b lattice vectors of the crystal lattice according to (b). The length of b is equal to the fcc volume lattice constant of FeS_2). Figure reprinted with permission from Ref. [27].

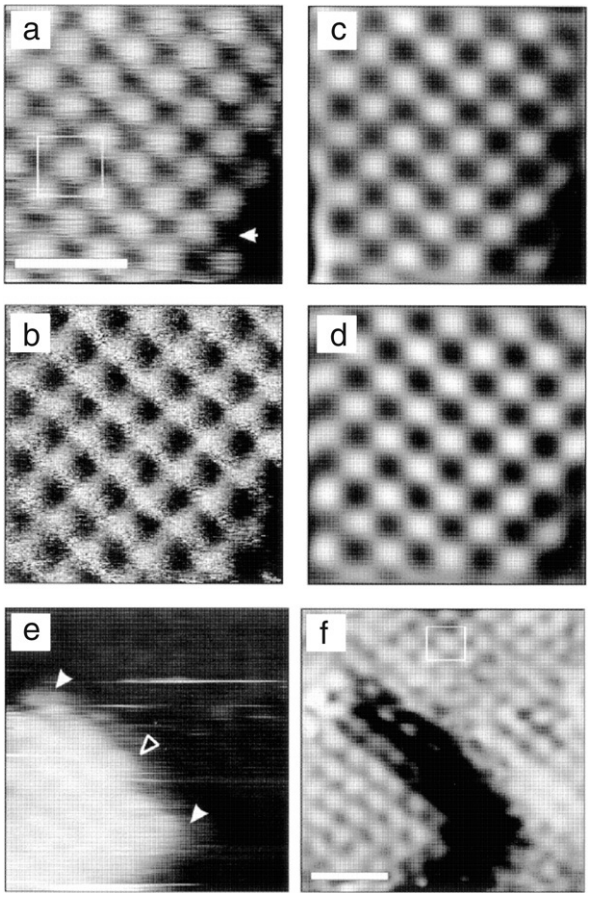

Fig. 4. Atomic-scale raw topographic (a) and current (b) UHV STM images of in-vacuum cleaved pyrite {100}. Image edges are roughly aligned with crystallographic axes of the single crystal sample. The *z* direction is perpendicular to the page. The images in (c) and (d) are low pass FFT filtered images of (a) and (b), respectively. The scale bar represents 10 Å in all the images. The lower right corner of (a) shows a half unit cell high step edge. The solid white arrow in (a) points to a corner site in the step edge. The tunneling conditions for (a–d) were −0.2 V bias and 2 nA setpoint current. Two terraces separated by a half unit cell high step are shown in topographic (e) and current (f) images collected in a different area from (a–d). Solid and outlined white arrows in (e) point to corner and kink sites along the step edge, respectively. The face-centered cubic surface cell (with some unavoidable image distortion) is outlined in (f). The step edge runs along ⟨11⟩ surface directions. The tunneling conditions were −0.1 V bias and 1.4 nA setpoint current. Images (e) and (f) are FFT filtered. Figure reprinted with permission from Ref. [28].

Fourier transform infrared spectroscopy (ATR-FTIR) experiments that rely on the adhesion of a high surface area solid to the ATR crystal. Preparation of the powder before such experiments generally includes the exposure of the as-received powder to water at a pH near 2, that effectively removes the oxide coating intrinsic to powder that has been exposed to the ambient atmosphere [25].

Pyrite powder has generally been produced by the crushing or grinding of large grains or surfaces of pyrite, or by the hydrothermal synthesis of pyrite. The latter method [26], which generally relies on the production of pyrite from an FeS precursor

Fig. 5. Topographic UHV STM images collected using a 1 V sample bias and 1 nA setpoint current showing pyrite cleavage surface microtopography. The scale bars represent 100 nm. The cubic axes are approximately aligned with the image edges. Unit cell high steps run along primarily ⟨10⟩ (a, d), ⟨10⟩ and ⟨11⟩ (b), and ⟨11⟩ (c) directions. Areas with a high step density were also commonly found as shown in (d). Less frequently, curved unit cell high steps were found (e). Figure reprinted with permission from Ref. [28].

at high pressure and temperature, results in a very fine grain material, having particle sizes down to a micron or less.

2.2.2. Cleaved surfaces

Due to conchoidal fracture, surfaces formed by the cleavage of large pyrite samples are macroscopically rough. The advantage of cleavage, however, is the generation of clean surfaces for vacuum-based studies in a straightforward manner. Cleavage of pyrite cubes along {100} planes has generally been the method of choice for photoelectron and probe microscopy studies of pyrite surfaces, which will be detailed later. While these fractured surfaces have visually rough surfaces, both low energy electron diffraction (LEED) [27] (Fig. 3) and scanning tunneling microscopy (STM) [28] (see Figs. 4 and 5) characterization have shown the retention of relatively flat {100} domains coexisting with the overall rough morphology of such surfaces.

2.2.3. Growth surfaces

As-grown surfaces obtained from natural pyrite cubes have also been used for surface science studies. Similar to pyrite powder that has been exposed to ambient atmosphere, as-grown surfaces of pyrite exhibit significant oxidation and the presence of adventitious carbon. To generate oxide-free surfaces, Strongin and coworkers [29–31] have prepared such surfaces by rinsing with pH 2 water. This treatment generates an oxide-free surface with a surface stoichiometry similar to surfaces produced by cleavage. High resolution photoelectron spectroscopy (PES) of these surfaces suggests that this preparation may result in a slightly higher surface concentration of polysulfides [29].

In addition to acid-pretreatment, Chaturvedi et al. [32] have shown that as-grown pyrite surfaces can be cleaned in vacuum by cycles of low energy ion bombardment and annealing. The advantage of such a preparation technique is the ability to generate a reproducible surface that can be used in a series of experiments. Specifically, repeated cycles of 200 eV He^+ bombardment and annealing (near 573 K) generated surfaces that were generally free of oxygen and carbon contamination. Atomic force microscopy (AFM) studies [33] have shown that as-grown surfaces treated by this method are rather rough, as seen in Fig. 6 but are presumably similar to the structure of the as-grown surfaces existing in the environment.

Fig. 6. UHV STM topographic image of an in-vacuum cleaned pyrite {100} growth surface. The mounds on the surface are between 1.5 and 4 nm in height. Tunneling conditions: +1 V bias and 1 nA tunneling current. Figure reprinted with permission from Ref. [33].

2.2.4. Pyrite thin films

Thin pyrite films have been prepared by a number of different techniques in part for their potential application in solar cell technology. By far the most common technique has been the sulfurization of an Fe thin film [34–58]. The Fe films are prepared by a variety of techniques, including thermal evaporation, flash evaporation and sputtering. The subsequent sulfurization is performed by thermal annealing of the film in a sulfur atmosphere. Other techniques involve the direct deposition of FeS_2 by sputtering [59,60], and flash evaporation [61–63] which may then be followed by annealing in a sulfur atmosphere. Another popular technique is chemical vapor deposition (CVD) [64–76] which allows vapor phase precursors to deposit onto a substrate